Low temperature matrix-isolation and solid state vibrational spectra of tetrazole

Susana C. S. Bugalho,[a] Ermelinda M. S. Maçôas,[a] M. Lurdes S. Cristiano[b] and Rui Fausto*[a]

[a] *Department of Chemistry (CQC), University of Coimbra, 3004-535 Coimbra, Portugal*
[b] *Department of Chemistry (UIQB), University of Algarve, 8000-117 Faro, Portugal*

Received 12th April 2001, Accepted 8th June 2001
First published as an Advance Article on the web 19th July 2001

Infrared spectra of tetrazole (CN_4H_2) isolated in an argon matrix ($T = 10$ K) and in the solid state (at room temperature) were investigated. In the crystalline phase, tetrazole exists in its 1*H*-tautomeric form and new assignments of the vibrational spectra (both infrared and Raman) of this phase are presented. The infrared spectrum of the matrix-isolated monomeric form of tetrazole is now reported and assigned for the first time, showing essentially the expected signature of the 2*H*-tetrazole tautomer. From relative intensities of the infrared bands ascribable to the two tautomers, the amount of the 1*H*-tautomer in the argon matrix was estimated to be *ca.* 10% of the most stable tautomer. Assuming that gas-phase relative populations of the two tautomers could be efficiently trapped in the argon matrix during deposition, the energy difference between 1*H*- and 2*H*-tetrazole (ΔE_{1H-2H}) was then obtained. The experimental value, $\Delta E_{1H-2H} = 6.95 \pm 1.50$ kJ mol^{-1}, now determined for the first time, compares fairly well with the theoretical predictions for the molecule in vacuum (*e.g.*, the zero point vibrational energy corrected energy difference obtained at the B3LYP/6–31G* level of theory is 9.96 kJ mol^{-1}).

Introduction

Tetrazole (CN_4H_2) and its derivatives attracted much attention owing to their practical applications. The tetrazolic acid fragment, $-CN_4H$, has similar acidity to the carboxylic acid group, $-CO_2H$, and is almost isosteric with it, but is metabolically more stable.[1] Hence replacement of $-CO_2H$ groups by $-CN_4H$ groups in biologically active molecules is a research area of major interest.[2] Indeed, the number of patent claims and publications related to medicinal uses of tetrazoles continue to grow rapidly and cover a wide range of applications: tetrazoles have been found to exhibit antihypertensive, antiallergic and antibiotic activity,[3–5] and they are currently used, for example, as anticonvulsants[6] and in cancer and AIDS treatment.[7,8] Tetrazoles are also applied in agriculture, as plant growth regulators, herbicides and fungicides,[9] as stabilizers in photography and photoimaging[10] and as gas-generating agents for airbags.[11]

From a more fundamental point of view, tetrazole is also a particularly interesting molecule, since it has been shown to exhibit tautomerism (Fig. 1). In the crystalline phases, tetrazole was found to exist exclusively as its 1*H*-tautomer.[12–14] On the other hand, in solution, 1*H*- and 2*H*-tautomers coexist, the population of the most polar 1*H*- form increasing with increasing polarity of the solvent.[15,16] The solvent effects on the tautomeric equilibrium were evaluated theoretically through the self-consistent reaction field (SCRF) model[17] and, in agreement with the experimental findings, it was predicted that 2*H*-tetrazole would be the lowest energy tautomer in media with dielectric constants smaller than *ca.* 7, whereas in media with larger dielectric constants a reversal of energy takes place and 1*H*-tetrazole becomes the tautomeric ground state.[17]

In the gaseous phase, the existence of 1*H*-tetrazole was suggested by microwave spectroscopy,[18] but not in studies using other techniques, such as photoelectron spectroscopy[19] or mass spectrometry.[20] Theoretical studies undertaken at different levels of approximation consistently predicted the 2*H*-tautomer as the most stable species in vacuum,[17,21–23] with the calculated energy difference between 1*H*-tetrazole and the most stable form ranging from 3.33 kJ mol^{-1} (B3LYP/3–21G*) to 12.13 kJ mol^{-1} (B3LYP/6-311++G**).[17]

Since the existence of 1*H*-tetrazole in the gaseous phase could not be proved experimentally (even though theory seems to indicate that it should be present as a minor component in the gas-phase tautomeric equilibrium at temperatures near room temperature), we decided to study tetrazole by matrix-isolation Fourier transform infrared spectroscopy, taking advantage of the unique features of this technique. The main strategy followed in the present study relies on the fact that, usually, matrix isolation enables one to trap efficiently, in the low temperature matrix, the gas-phase equilibrium existing in the sample vapour prior to deposition.[24–26] Then, taking advantage of the high spectral resolution typical of matrix-isolation spectroscopic experiments (usually a few tenths of 1 cm^{-1}), ideal conditions can be achieved to identify spectroscopic features due to the different species trapped in the matrix, and from these estimate the composition of the deposited gaseous mixture. To support the experimental observations further, the spectroscopic data were systematically compared with the predicted spectra of the two tautomers of tetrazole, calculated at a convenient level of theory (B3LYP/6-31G*).

Finally, the infrared and Raman spectra of the crystalline room temperature phase of tetrazole were also revisited in this study and revised assignments are presented.

Experimental and computational methods

Tetrazole (Aldrich, 99+%) was preliminarily purified by multiple recrystallization from ethanol. Solid state spectra were obtained in KBr pellets (infrared) or in Kimax glass capillary tubes of *ca.* 0.8 mm id (Raman), at room temperature. In the matrix-isolation experiments, a glass vacuum system and

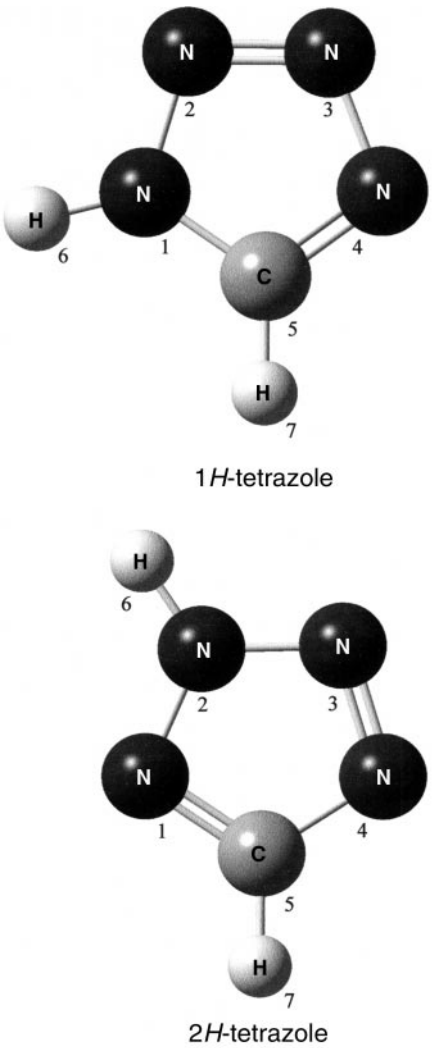

Fig. 1 1*H*- and 2*H*-tautomers of tetrazole, with atom numbering.

standard manometric procedures were used to deposit the matrix gas (argon, Air Liquid, 99.9999%), which was used without further purification. The gas deposition rate during sample preparation was *ca.* 10 mmol h^{-1}. Tetrazole was co-deposited from a specially designed Knudsen cell with shut-off possibility, the principal component of which is an SS-4BMRG micrometer valve (NUPRO). The cell has two independent thermostatable parts, the valve nozzle and the sample compartment. This design permits more precise control of the saturated gas pressure over the liquid and a better metering function of the valve. Further details of the experimental set up can be found elsewhere.[27]

The infrared spectra, in the range 4000–500 cm^{-1}, were obtained using a Mattson (Infinity 60AR Series) or a Bomem (MB104) Fourier transform spectrometer equipped with a deuterated triglycine sulfate (DTGS) detector and Ge/KBr or Zn/Se beamsplitters. Data collection was performed with 1 cm^{-1} spectral resolution. All matrix-isolation experiments were carried out on the basis of an APD Cryogenics closed-cycle helium refrigeration system with a DE-202A expander. Necessary modifications of the sample compartment of the spectrometer were made in order to accommodate the cryostat head and allow efficient purging of the instrument with a stream of dry air to remove water and CO_2 vapours.

Raman spectra were obtained using a Spex 1403 double monochromator spectrometer (focal length 0.85 m, aperture *f*/7.8) equipped with 1800 grooves mm^{-1} holographic gratings (reference 1800-1SHD). Radiation of 514.5 nm from an Ar^+ laser, adjusted to provide 220 mW power at the sample, was used for excitation. Detection was effected using a thermoelectrically cooled Hamamatsu R928 photomultiplier. The spectrum was recorded using increments of 1 cm^{-1} and integration times of 1 s.

Theoretical calculations were performed with the GAUSSIAN 98 program package[28] using the Becke-style three-parameter density functional with the Lee–Yang–Parr correlation functional (B3LYP)[29–31] and the 6-31G* basis set.[32] Molecular geometries were fully optimized by the force gradient method using Benny's algorithm[33] using the tight built-in convergence criteria. The precise nature of the optimized stationary points was determined by analysis of the corresponding Hessian matrices.

The calculated (B3LYP/6-31G*) harmonic wavenumbers were scaled down using a single scale factor (0.9614[34]). The mean relative error in the fitted wavenumbers was less than 1.5%. Normal coordinate analysis was undertaken using the programs TRANSFORMER, BUILD-G and VIBRAT,[35] which were interfaced with GAUSSIAN 98.

Results and discussion

Molecular structures and energies

Table 1 summarizes the structural and energetic results of the theoretical calculations. In consonance with previously published results,[17,21–23] the B3LYP/6–31G* calculations predict the 2*H*-tautomer of tetrazole to be more stable than the 1*H*-tautomer by 11.79 kJ mol^{-1}. When energies are corrected by zero-point vibrational energy contributions, the calculations predict $\Delta E_{1H-2H} = 9.96$ kJ mol^{-1}.

A detailed analysis of the molecular geometries of the two tautomers of tetrazole was made previously[17] and will not be repeated here. The B3LYP/6–31G* calculated geometries are similar to those reported previously[17,21–23] obtained with the highest level methods and agree fairly well with available experimentally obtained data (1*H*-tetrazole: X-ray; α-crystal[14]). The formal double bond, N2=N3, is considerably shorter than both the N1–N2 and N3–N4 bonds, indicating that there is considerable localization of charge within the ring. In agreement with expectations, the calculations also predict the C5=N4 bond to be shorter than the C5–N1 bond in monomeric 1*H*-tetrazole (see Table 1). However, in the α-crystalline state, the opposite trend was observed,[14] indicating that in the crystal the structural requirements to attain a more favourable intermolecular interaction geometry for H-bond formation play a relevant role in determining the overall structure of the tetrazole ring. In addition, since N4 acts as an H-bond acceptor, the increase in the C5=N4 bond length in the crystalline state is also in agreement with the occurrence of an electron charge migration from the C5=C4 bond towards the hydrogen bond upon hydrogen bond formation. On the other hand, the opposite effect can be expected to occur in the case of the C5–N1 bond, since N1 acts as an H-bond donor, thus justifying the observed shortening in this bond on going from the isolated monomer to the associated species in the crystal.

For 2*H*-tetrazole, there are no available experimental geometrical data, except rotational constants, obtained from microwave spectroscopic measurements in the gaseous phase.[18] It is clear from the results in Table 1 that in this phase 2*H*-tetrazole is the dominant tautomer, since the observed rotational constants are much closer to those calculated for this tautomer than for 1*H*-tetrazole (the same conclusion can also be extracted by comparing the experimentally determined dipole moment, 2.19 ± 0.05 D,[18] with those obtained from calculations, 5.34 and 2.27 D for 1*H*- and 2*H*-tetrazole, respectively). In agreement with the relative polarity of the two tautomers, the calculations predict a relatively more extensive electron delocalization within the ring for 2*H*- than for 1*H*-tetrazole. Hence the formal N–N single bonds are

Table 1 B3LYP/6–31G* calculated molecular geometries, rotational constants, energies and dipole moments and available experimental data for 1*H*- and 2*H*-tetrazole[a]

1*H*-tetrazole			2*H*-tetrazole		
Parameter	Exp.[14 b]	B3LYP/6-31G*	Parameter	Exp.[18 c]	B3LYP/6-31G*
Bond lengths					
N1–N2	133.2 ± 0.2	135.3	N1–N2		132.9
N2=N3	129.5 ± 0.3	129.2	N2–N3		132.9
N3–N4	134.6 ± 0.3	136.6	N3=N4		131.1
N1–C5	130.8 ± 0.2	134.7	N1=C5		132.9
N4=C5	131.5 ± 0.2	131.5	N4–C5		135.7
N1–H6	81 ± 5	101.1	N2–H6		101.2
C5–H7	88 ± 4	108.0	C5–H7		107.9
Bond angles					
N1–N2=N3	106.0 ± 0.2	105.9	N1–N2–N3		115.0
N2=N3–N4	110.5 ± 0.2	111.4	N2–N3=N4		105.3
N2–N1–C5	109.2 ± 0.2	108.6	N2–N1=C5		100.2
N3–N4=C5	105.5 ± 0.2	105.6	N3=N4–C5		106.4
N1–C5=N4	108.8 ± 0.2	108.4	N1=C5–N4		113.1
N2–N1–H6	123 ± 3	120.3	N1–N2–H6		122.7
C5–N1–H6	127 ± 3	131.1	N3–N2–H6		122.3
N1–C5–H7	127 ± 3	124.8	N1=C5–H7		123.1
N4=C5–H7	124 ± 3	126.7	N4–C5–H7		123.8
Rotational constants					
A		10 496.58		10 667.32 ± 0.18	10 691.16
B		10 308.21		10 310.91 ± 0.18	10 287.61
C		5200.77		5240.37 ± 0.15	5242.75
Energies					
E		−678 037.81			−678 049.60
ZPVE		123.26			125.09
ΔE[d]		9.96			0.00
Dipole moments					
μ		5.34		2.19 ± 0.05	2.27

[a] Bond lengths in pm; angles in degrees; rotational constants in MHz; energies in kJ mol^{-1}; dipole moments in debye (1 D = 3.335 64 × 10^{-30} C m); ZPVE = zero point vibrational energy. See Fig. 1 for atom numbering. [b] X-ray data for α-crystal (triclinic). [c] Microwave spectroscopic results. [d] Energy relative to the most stable tautomer.

calculated to be shorter in 2*H*- than in 1*H*-tetrazole, whereas the formal N=N and C=N double bonds are predicted to be longer in 2*H*-tetrazole. This increased electron delocalization within the ring is certainly a factor leading to a lower energy of the monomeric 2*H*- than the 1*H*-tautomer, in agreement with both the experimental findings and the theoretical predictions.

Matrix-isolation FTIR studies

The matrix isolation infrared spectra of tetrazole trapped in an argon matrix are shown in Fig. 2, where trace (A) corresponds to the spectrum obtained immediately after deposition, with the cold substrate temperature kept constant at 10 K, trace (B) is the spectrum obtained after annealing at 20 K and trace (C) is the difference spectrum [(A) − (B)]. The experimental spectrum (A) is compared with the B3LYP/6–31G* predicted spectra for 1*H*- and 2*H*-tetrazole in Fig. 3. Table 2 contains the proposed assignments of the experimentally observed spectra and the results of the theoretical vibrational calculations [calculated frequencies and intensities and potential energy distributions (PEDs)].

The spectrum shown in Fig. 2(A) is dominated by bands due to monomeric tetrazole, although several less intense bands due to aggregated species could also be observed. Upon annealing of the matrix at 20 K [Fig. 2(B)], the intensities of the bands due to aggregates increase. This increase in the population of the aggregates is clearly revealed in the difference spectrum Fig. 2(C): the bands pointing up are due to monomeric tetrazole, whereas those pointing down originate in the aggregates. Hence the annealing experiments allowed a reliable identification of the spectroscopic features due to the monomeric species.

The next step was the assignment of the bands originating in monomeric tetrazole. In order to do this, the observed spectrum was compared with the calculated spectra (B3LYP/6-31G*) for the two tautomers. It can easily be seen from the results in Fig. 3 that the experimental spectrum shows essentially the expected signature of the 2*H*-tetrazole tautomer. However, bands due to the second tautomer can also be

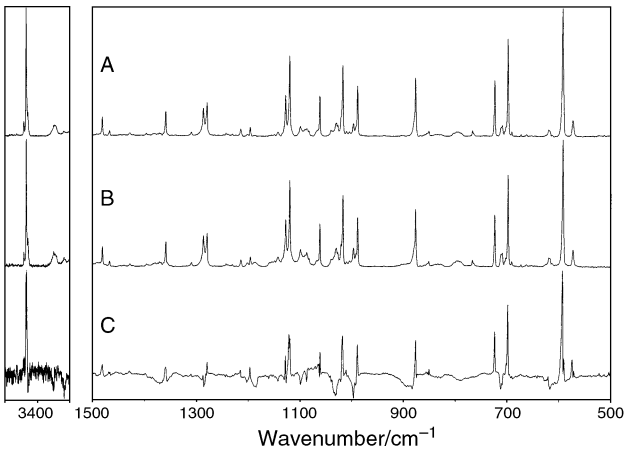

Fig. 2 Infrared spectra of tetrazole trapped in an argon matrix (in each spectral region shown, absorbances were normalized to that of the most intense band). (A) Spectrum obtained immediately after deposition, with the cold substrate temperature kept constant at 10 K; (B) spectrum obtained after annealing of the matrix at 20 K; (C) difference spectrum [(A) − (B)]. In the difference spectrum, bands pointing down are due to aggregates and those pointing up are due to monomeric species.

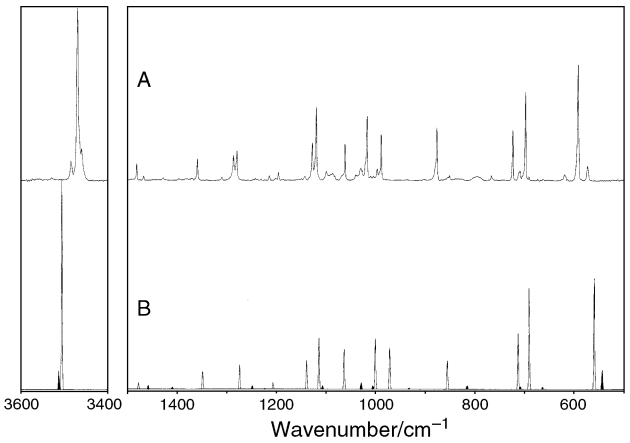

Fig. 3 Comparison of (A) the experimental infrared spectrum of tetrazole trapped in an argon matrix, obtained immediately after deposition (temperature prior to deposition 363.15 K), with (B) the simulated spectrum generated from the B3LYP/6-31G* predicted spectra for 1*H*- and 2*H*-tetrazole (in the simulated spectrum, bands due to 1*H*-tetrazole are shown in black; the calculated intensities for 1*H*-tetrazole were multiplied by 0.1, in order to reproduce the observed intensity ratio of bands due to the tautomers).

clearly observed in this spectrum, testifying to the presence of 1*H*-tetrazole in the gaseous phase prior to matrix deposition.

The most intense bands for both tautomers, as predicted by the calculations, should correspond to the ν(N–H) stretching mode and the γ(N–H) out-of-plane bending vibration (see Table 2). In 1*H*-tetrazole, these modes are predicted to occur at higher and lower frequencies, respectively, when compared with the same vibrations in 2*H*-tetrazole (3512.0 and 543.4 cm^{-1}, *vs.* 3504.7 and 559.4 cm^{-1}). Accordingly, the observed bands due to 1*H*-tetrazole appear at 3484.3 cm^{-1}, ν(N–H) and 573.4 cm^{-1}, γ(N–H), whereas those ascribable to the most populated 2*H*-tautomer correspond to the intense features observed at 3468.8 cm^{-1}, ν(N–H) and 592.6 cm^{-1}, γ(N–H).

From the relative intensities of the infrared bands ascribable to the two tautomers, the amount of the 1*H*-tautomer in the argon matrix can be estimated to be *ca.* 10% of that of the most stable tautomer. Assuming that gas-phase relative populations of the two tautomers (T = 363.15 K) could be efficiently trapped in the argon matrix during deposition, the enthalpy difference between 1*H*- and 2*H*-tetrazole (ΔH_{1H-2H}) can then be obtained. The experimental value, ΔH_{1H-2H} = 6.95 ± 1.50 kJ mol^{-1}, now determined for the first time, compares fairly well with the theoretical predictions for the mol-

Table 2 Calculated and observed vibrational frequencies, intensities and potential energy distributions (PED) for 2*H*- and 1*H*-tetrazole[a]

		Calculated (B3LYP/6-31G*)			Observed				
					Argon, 10 K		Crystal		
Approximate description	Symmetry	ν (scaled)	I^{IR}	I^{R}	ν	I^{IR}	ν^{IR}	ν^{R}	PED[b]
2*H*-Tetrazole									
ν(N–H)	A′	3504.7	91.0	100.7	3468.8	100.0			ν(N–H) 100
ν(C–H)	A′	3184.7	0.1	76.1	n.o				ν(C–H) 100
ν(C=N)	A′	1477.9	2.5	2.2	1481.6	9.6			ν(C=N) 33, δ(N–H) 35, δ(C–H) 18
δ(N–H)	A′	1348.6	7.9	8.6	1359.2	12.5			δ(N–H) 44, δ(C–H) 26, ν(C=N) 24, ν(C–N) 12, δ(NNN as.) 12
ν(C–N)	A′	1274.0	10.2	3.9	1279.6	17.0			ν(C–N) 27, ν(C=N) 31, ν(N1–N2) 17, δ(C–H) 13
ν(N=N) FR with 2γN–H	A′	1206.8	3.1	17.6	1214.3 1196.1	2.8 4.8			ν(N=N) 81, ν(N1–N2) 12
ν(N1–N2)	A′	1139.1	11.6	5.8	1127.9	21.3			ν(N1–N2) 47, ν(C–N) 26, δ(NNN as.) 19, δ(NCN) 19
δ(C–H)	A′	1114.3	21.9	4.0	1119.8	42.2			δ(C–H) 31, ν(C–N) 23, ν(N2–N3) 12
ν(N2–N3)	A′	1063.4	18.2	6.1	1061.8	20.8			ν(N2–N3) 76
δ(NNN as.)	A′	1000.6	22.4	2.2	1017.4	37.1			δ(NNN as.) 52, ν(N1–N2) 12
δ(NCN)	A′	971.7	18.6	3.3	989.0	26.4			δ(NCN) 78
γ(C–H)	A″	855.4	12.7	1.2	876.8	30.5			γ(C–H) 90
γ(ring 1)	A″	713.0	22.9	0.2	724.0	29.1			γ(ring 1) 97
γ(ring 2)	A″	690.8	42.8	0.1	698.4	51.0			γ(ring 2) 73
γ(N–H)	A″	559.4	51.4	1.1	592.6	66.9			γ(N–H) 88
1*H*-Tetrazole									
ν(N–H)	A′	3512.0	79.5	101.5	3484.3	11.1	[c]	[c]	ν(N–H) 100
ν(C–H)	A′	3182.3	0.8	72.5	n.o		3158.3	3158.5	ν(C–H) 100
ν(C=N) + δ(N–H)	A′	1458.4	18.4	2.8	1467.6	2.5	1524.6	1530.3	ν(C=N) 48, δ(N–H) 28, δ(C–H) 20
ν(C–N)	A′	1409.8	9.2	6.5	1428.2	1.3	1451.6 1444.8	1448.9	ν(C–N) 54, δ(N–H) 32, δ(C–H) 20, ν(C=N) 17, δ(NNN as.) 16
ν(N=N)	A′	1248.8	15.6	18.9	1242.7	1.2	1259.3	1259.9	ν(N=N) 87
δ(N–H) + ν(C=N)	A′	1223.4	3.1	4.9	n.o.		1145.1	1144.5	δ(N–H) 20, ν(C=N) 32, δ(C–H) 20, ν(N1–N2) 11
δ(C–H)	A′	1107.1	15.6	7.9	1090.3	[d]	1085.3	1086.1	δ(C–H) 27, ν(C–N) 30
ν(N3–N4)	A′	1029.2	28.4	2.6	1040.6	3.1	1049.6	1048.6	ν(N3–N4) 41, δ(NNN as.) 34, δ(NCN) 27, δ(N–H) 18, ν(C–N) 13
ν(N1–N2)	A′	1005.6	16.9	4.9	1010.5	2.6	1015.1 999.2	1013.7	ν(N1–N2) 81, ν(N3–N4) 14
δ(NCN)	A′	972.1	0.2	2.6	n.o.		951.5	947.2	δ(NCN) 72
δ(NNN as.)	A′	932.7	4.3	2.0	938.4	0.1	937.1	n.o.	δ(NNN as.) 47, ν(N3–N4) 47, δ(C–H) 12
γ(C–H)	A″	815.5	17.0	0.8	851.2	2.9	907.2	905.4	γ(C–H) 90
γ(ring 1)	A″	708.6	7.9	<0.1	n.o.		722.4	n.o.	γ(ring 1) 92
γ(ring 2)	A″	663.8	8.2	0.4	673.7	1.1	663.1	662.5	γ(ring 2) 83
γ(N–H)	A″	543.4	91.8	1.1	573.4	8.4	884.4	n.o.	γ(N–H) 74, γ(ring 2) 21

[a] Frequencies in cm^{-1}. ν, Stretching; δ, in-plane bending; γ, out-of-plane bending; as., asymmetric; FR, Fermi resonance; n.o., not observed. See Fig. 1 for atom numbering. Calculated infrared intensities (I^{IR}) in km mol^{-1}; calculated Raman activities (I^{R}) in Å^4 Da^{-1}. Experimental intensities are peak intensities, normalized (to 100) to the most intense band. [b] Only PED contributions larger than 10% are presented. [c] Very broad and complex band (see Fig. 4 or 5 and discussion in the text). [d] Superimposed with bands due to aggregated species.

ecule in vacuum (the zero point vibrational energy corrected energy difference obtained at the B3LYP/6–31G* level of theory is 9.96 kJ mol^{-1}).

A few further comments on the data in Fig. 2 and Table 2 for the monomeric species can be made: (i) the general agreement between the calculated and observed spectra for the two tautomers is excellent with respect to both frequencies and relative intensities, stressing the good capabilities of the B3LYP/6-31G* calculations in predicting vibrational spectra of this type of molecule and opening up good prospects for the detailed study of more complex tetrazole molecules by this approach; (ii) in both tautomers, most of the vibrations show a considerable mixture of coordinates, this being particularly noticeable for the CN stretching and CH and NH in-plane bending coordinates, which have significant contributions to several normal modes (see PEDs in Table 2); and (iii) taking into consideration the relative energy of the two tautomers of tetrazole, the energy barriers for tautomerization could be expected to be large enough to be overcome in the temperature range covered by the annealing experiments (Barnes[36] estimated that, at 20 K, observation of changes in relative populations in matrix-isolated molecules would require an energy barrier lower than 5 kJ mol^{-1}); these expectations were confirmed by the experiments, since annealing of the matrix did not lead to any changes in the relative intensities of the bands due to the two tautomers.

Solid state FTIR and Raman studies

The infrared and Raman spectra of the room temperature crystalline phase (α-crystal[14]) were first reported by Sokolova *et al.*[37] over 25 years ago. In that study, the molecule was correctly assumed to exist within the crystal as the 1*H*-tautomer, and an empirical force field was used to interpret the experimental observations and help band assignments. Recently, room temperature crystalline tetrazole was submitted to a new investigation by FTIR and Raman spectroscopy, complemented by theoretical calculations undertaken at the B3P86/6-311G** level of theory,[38] and new assignments were proposed. However, the analysis of the spectra made in this more recent study did not take into consideration the previously reported X-ray structure of crystalline tetrazole[14] (apparently the authors ignored the existence of X-ray data for this compound, since they explicitly state that "For tetrazole we found only calculated structures") and they interpreted the spectra on the basis of simultaneous presence in the crystal of both 1*H*- and 2*H*-tautomers. In the present study, a reviewed assignment of the spectra of crystalline tetrazole was made, taking into consideration (i) the information now obtained by matrix-isolation spectroscopy for the monomeric forms, (ii) the knowledge on the structure of crystalline tetrazole, previously obtained by X-ray crystallography,[14] and (iii) the results of the theoretical vibrational calculations.

Fig. 4 and 5 show the infrared and Raman spectra of crystalline tetrazole, respectively, obtained at room temperature. The proposed assignments are given in Table 2.

The exact nature of the crystalline phase under study could be easily confirmed by analysis of the low frequency spectral region of the Raman spectrum. Below 200 cm^{-1}, the observed bands (108 cm^{-1} with shoulder in the 112–120 cm^{-1} region, 137 and 168 cm^{-1} with shoulder at 180 cm^{-1}) are ascribable to external optical librations and the results now obtained are identical with those previously reported by Baglin,[39] which demonstrated that the observed profile is consistent with the *P*1 space group (characteristic of the α-phase triclinic crystalline variety).

The assignment of several bands in both the infrared and Raman spectra of crystalline tetrazole could now be made in a relatively straightforward way, taking advantage of the information obtained from the matrix-isolation experiments for monomeric 1*H*-tetrazole and considering the results of the vibrational calculations. Since in the crystal intermolecular interactions involve mainly the N–H fragment, it could be expected that those modes with predominant contributions from coordinates associated with this group should be more affected by intermolecular interactions, and deserve further comments here.

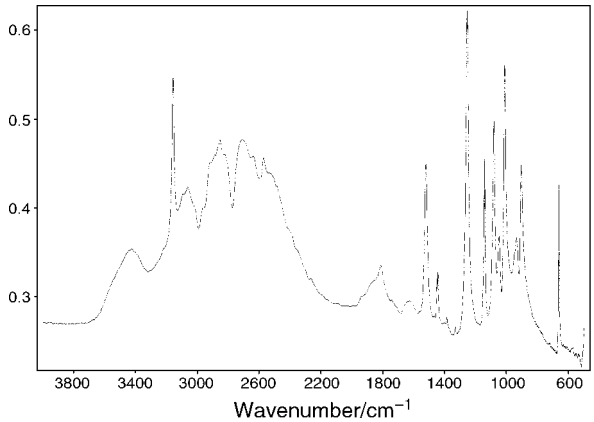

Fig. 4 Infrared spectrum of crystalline (α-phase) tetrazole, at room temperature.

The ν(N–H) stretching and γ(N–H) out-of-plane bending modes are expected to be those showing larger frequency shifts on going from the monomeric species to the crystalline state. In the first case, a shift to lower frequencies is expected, owing to the participation of the N–H group in intermolecular H-bonding, whereas in the case of the out-of-plane bending mode, a shift to higher frequencies is expected, due to both H-bonding and the crystal packing forces (the crystal packing is graphitic like[14]).

Accordingly, in the infrared spectrum ν(N–H) can be easily assigned to the broad complex set of intense bands observed from *ca.* 3500 to *ca.* 2300 cm^{-1} [the narrow band at 3158 cm^{-1} is due to ν(C–H)]. The observed pattern is typical of ν(N–H) vibrations participating in strong H-bond interactions and being involved in multiple Fermi resonance interactions with overtones and combination tones of lower frequency fundamental vibrations.[40] In the Raman spectrum, ν(N–H) is predicted to be relatively much less intense, and is ascribed to a set of weak broad bands whose main intensity is concentrated in the 3200–2900 cm^{-1} region.

On the other hand, the assignment of the γ(N–H) out-of-plane bending was not so easily made. Being directly affected by intermolecular interactions, we could expect this mode to give rise to relatively broad bands. Thus, taking into consideration its low predicted Raman intensity (see Table 2), we did

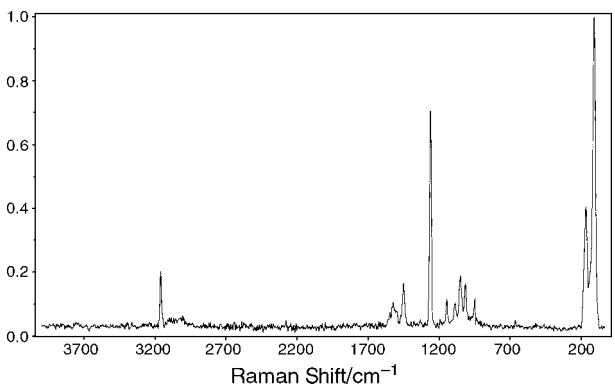

Fig. 5 Raman spectrum of crystalline (α-phase) tetrazole, at room temperature (intensities were normalized to that of the most intense band).

not expect to be able to observe any spectral feature ascribable to γ(N–H) in the Raman spectrum. On the other hand, the predicted infrared intensity is large and it should be observed. However, at a first inspection of the infrared spectrum, no candidate band to be assigned to γ(N–H) could be identified. Indeed, below 1000 cm^{-1} [it did not appear to be reasonable to expect γ(N–H) to appear at a frequency larger than this value], the bands at 663.1, 722.4, 937.1 and 951.5 cm^{-1} were undoubtedly ascribed to γ(ring 2), γ(ring 1), δ(NNN as.) and δ(NCN), respectively [appearing in the spectra of matrix isolated 1*H*-tetrazole or being predicted to occur in the monomeric form at similar frequencies: 673.7, 708.6 (calculated), 938.4 and 972.1 cm^{-1} (calculated)], whereas the band observed at 907.2 cm^{-1} is ascribable to γ(C–H), which, as expected, appears slightly shifted to higher frequencies in comparison with the observed value for the isolated molecule (851.2 cm^{-1}). A more detailed inspection of the spectrum, however, allowed the identification of the feature originating in γ(N–H). Fig. 6 shows the results of band deconvolution analysis of the spectroscopic profile in the 1300–750 cm^{-1} spectral region, where a broad intense band could easily been observed, centred at 884.4 cm^{-1}, which fulfil all expected characteristics for assignment to the γ(N–H) mode. The frequency shift, when compared with the observed frequency for the monomer (573.4 cm^{-1}), is *ca.* 300 cm^{-1}, and is of the same order of magnitude as that observed[41] for the τ(O–H) torsional vibration in methyl glycolate ($CH_2OHCOOCH_3$) on going from the matrix-isolated monomeric species (303 cm^{-1}) to the crystalline state (652, 570 cm^{-1}).

The effects of intermolecular interactions on the vibrations with significant contributions of δ(N–H) are considerably more complex, since this coordinate is extensively coupled with other coordinates. However, relatively important shifts to higher frequencies were observed on going from the isolated molecule situation to the crystal in the case of the modes which, in the infrared spectrum of the crystal, give rise to the bands at 1524.6 and 1451.6/1444.8 cm^{-1} [approximately described as ν(C=N) + δ(N–H) and ν(C–N)] that show PED contributions from δ(N–H) of 28 and 32%, respectively, for the isolated molecule (see Table 2). On the other hand, the third vibration, showing a significant contribution from the δ(N–H) coordinate for the monomer (20%), is assigned to the infrared band appearing at 1145.1 cm^{-1} and shows a shift to lower frequencies when compared with the predicted vibration for the monomer (1223.4 cm^{-1}; this vibration could not be observed in the spectrum of the matrix-isolated monomer owing to its low intensity). These results seem to indicate that relatively important changes in the mode compositions occur for these three vibrations on going from the monomer to the crystalline state, with the relative contribution of the δ(N–H) coordinate increasing in the case of the two first modes and decreasing in the last.

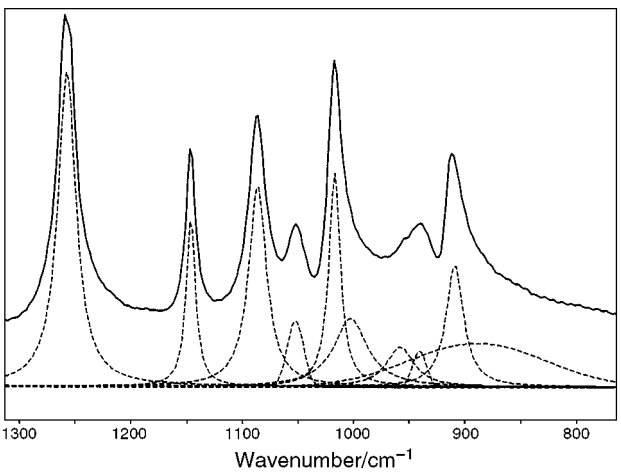

Fig. 6 Results from band-fitting analysis for the 1300–750 cm^{-1} region of the room temperature infrared spectrum of crystalline (α-phase) tetrazole. In the simulation, the Grams/32 AI 6.0 (Galactic Industries, Salem, NH, USA, 2000) was used, with Gaussian–Lorentzian type functions selected as adjusting functions.

Conclusion

Matrix-isolated infrared spectroscopy supported by theoretical predictions undertaken at the B3LYP/6-31G* level of theory allowed, for the first time, unequivocal observations of the two tautomers of tetrazole which are present in the gaseous phase. It was shown that in the gaseous phase, 2*H*-tetrazole is more stable than 1*H*-tetrazole by *ca.* 6.95 kJ mol^{-1} (B3LYP/6-31G* calculated value: 9.96 kJ mol^{-1}), corresponding to a relative population of 10 : 1 at $T = 363.15$ K. A detailed assignment of the observed infrared spectra of matrix-isolated monomeric tetrazole (both 1*H*- and 2*H*-tautomers) was carried out taking into consideration also the results of the theoretical vibrational calculations, including normal coordinate analysis.

In addition, the infrared and Raman spectra of crystalline tetrazole were reviewed. It was shown that the spectra of the crystal (α-form; triclinic variety) could be explained on the basis of the exclusive existence of 1*H*-tetrazole in this phase, in agreement with the available X-ray data.[12,14] These results improve on the vibrational assignments made previously,[38] where the simultaneous presence in the crystal of both 1*H*- and 2*H*-tautomers of tetrazole was assumed.

Acknowledgement

The authors thank the Portuguese Science Foundation (FCT) for financial support (Research Project PRAXIS/P/QUI/10137/1998).

References

1 H. Singh, A. S. Chawla, V. K. Kapoor, D. Paul and R. K. Malhotra, *Prog. Med. Chem.*, 1980, **17**, 151.
2 K. Noda, Y. Saad, A. Kinoshita, T. P. Boyle, R. M. Graham, A. Husain and S. S. Karnik, *J. Biol. Chem.*, 1995, **270**, 2284.
3 T. Mavromoustakos, A. Kolocouris, M. Zervou, P. Roumelioti, J. Matsoukas and R. Weisemann, *J. Med. Chem.*, 1999, **42**, 1714.
4 J. H. Toney, P. M. D. Fitzgerald, N. Grover-sharma, S. H. Olson, W. J. May, J. G. Sundelof, D. E. Vanderwall, K. A. Cleary, S. K. Grant, J. K. Wu, J. W. Kozarich, D. L. Pompliano and G. G. Hammond, *Chem. Biol.*, 1998, **5**, 185.
5 Y. Hashimoto, R. Ohashi, Y. Kurosawa, K. Minami, H. Kaji, K. Hayashida, H. Narita and S. Murata, *J. Cardiovasc. Pharmacol.*, 1998, **31**, 568.
6 A. Desarro, D. Ammendola, M. Zappala, S. Grasso and G. B. Desarro, *Antimicorb. Agents Chemother.*, 1995, **39**, 232.
7 Y. Tamura, F. Watanabe, T. Nakatani, K. Yasui, M. Fuji, T. Komurasaki, H. Tsuzuki, R. Maekawa, T. Yoshioka, K. Kawada, K. Sugita and M. Ohtani, *J. Med. Chem.*, 1998, **41**, 640.
8 A. D. Abell and G. J. Foulds, *J. Chem. Soc., Perkin Trans. 1*, 1997, **17**, 2475.
9 G. Sandmann, C. Schneider and P. Boger, *Z. Naturforsch. C: Biosci.*, 1996, **51**, 534.
10 G. I. Koldobskii, V. A. Ostrovskii and V. S. Poplavskii, *Khim. Geterotsikl. Soedin.*, 1981, **10**, 1299.
11 C. Zhao-Xu and X. Heming, *Int. J. Quantum Chem.*, 2000, **79**, 350.
12 W. C. McCrone, D. Grabar and E. Lieber, *Anal. Chem.*, 1957, **23**, 543.
13 N. Van der Putten, D. Heijdenrijk and H. Schenk, *Cryst. Struct. Commun.*, 1974, **3**, 321.
14 R. Goddard, O. Heinemann and C. Krüger, *Acta. Crystallogr., Sect. C: Cryst. Struct. Commun.*, 1997, **53**, 590.
15 R. N. Butler, V. C. Garvin, H. Lumbroso and C. Liègeois, *J. Chem. Soc., Perkin Trans. 2*, 1984, 721.
16 C. Zhaoxu and X. Heming, *J. Mol. Struct. (Theochem.)*, 1998, **453**, 65.
17 A. P. Mazurek and N. Sadlej-Sosnowska, *Chem. Phys. Lett.*, 2000, **330**, 212.

18 W. D. Krugh and L. P. Gold, *J. Mol. Spectrosc.*, 1974, **49**, 423.
19 A. Razynska, A. Tempczyk, E. Maslinski, J. Szafranek and Z. Grzonka, *J. Chem. Soc., Perkin Trans. 2*, 1983, 379.
20 M. H. Palmer, I. Simpson and J. R. Wheeler, *Z. Naturforsch, A: Phys. Phys. Chem. Kosmophys.*, 1981, **36**, 1246.
21 W. M. F. Fabian, *Z. Naturforsch., A: Phys. Sci.*, 1990, **45**, 1328.
22 B. S. Jursic and Z. Zdravkovski, *J. Mol. Struct.* (*Theochem.*), 1995, **337**, 9.
23 M. W. Wong, R. Leung-Toung and C. Wentrup, *J. Am. Chem. Soc.*, 1993, **115**, 2465.
24 S. G. Stepanian, I. D. Reva, E. D. Radchenko, M. T. S. Rosado, M. L. T. S. Duarte, R. Fausto and L. Adamowicz, *J. Phys. Chem. A*, 1998, **102**, 1041.
25 E. M. S. Maçôas, R. Fausto, J. Lundell, M. Pettersson, L. Khriachtchev and M. Räsänen, *J. Phys. Chem. A*, 2000, **104**, 11725.
26 E. M. S. Maçôas, R. Fausto, M. Pettersson, L. Khriachtchev and M. Räsänen, *J. Phys. Chem. A*, 2000, **104**, 6956.
27 I. D. Reva, S. Stepanian, L. Adamowicz and R. Fausto, *J. Phys. Chem. A*, 2001, **105**, 4773.
28 M. J. Frisch, G. W. Trucks, H. B. Schlegel, G. E. Scuseria, M. A. Robb, J. R. Cheeseman, V. G. Zakrzewski, J. A. Montgomery Jr., R. E. Stratmann, J. C. Burant, S. Dapprich, J. M. Millam, A. D. Daniels, K. N. Kudin, M. C. Strain, O. Farkas, J. Tomasi, V. Barone, M. Cossi, R. Cammi, B. Mennucci, C. Pomelli, C. Adamo, S. Clifford, J. Ochterski, G. A. Petersson, P. Y. Ayala, Q. Cui, K. Morokuma, D. K. Malick, A. D. Rabuck, K. Raghavachari, J. B. Foresman, J. Cioslowski, J. V. Ortiz, A. G. Baboul, B. B. Stefanov, G. Liu, A. Liashenko, P. Piskorz, I. Komaromi, R. Gomperts, R. L. Martin, D. J. Fox, T. Keith, M. A. Al-Laham, C. Y. Peng, A. Nanayakkara, C. Gonzalez, M. Challacombe, P. M. W. Gill, B. Johnson, W. Chen, M. W. Wong, J. L. Andres, C. Gonzalez, M. Head-Goron, E. S. Replogle and J. A. Pople, GAUSSIAN 98, Revision A.7, Gaussian, Pittsburgh PA, 1998.
29 A. D. Becke, *Phys. Rev. B: Condens. Matter*, 1988, **38**, 3098.
30 C. Lee, W. Yang and R. G. Parr, *Phys. Rev. B: Condens. Matter*, 1988, **37**, 785.
31 S. H. Vosko, L. Wilk and M. Nusair, *Can. J. Phys.*, 1980, **58**, 1200.
32 W. J. Hehre, R. Ditchefield and J. A. Pople, *J. Chem. Phys.*, 1972, **56**, 2257.
33 C. Peng, P. Y. Ayala, H. B. Schlegel and M. J. Frisch, *J. Comput. Chem.*, 1996, **17**, 49.
34 D. J. Defrees and A. D. McLean, *J. Chem. Phys.*, 1985, **82**, 333.
35 M. D. G. Faria and R. Fausto, *TRANSFORMER*, *BUILD-G and VIBRAT* (*Version 2.0*), Department of Chemistry, University of Coimbra, Portugal, 1997. (These programs incorporate several routines from programs GMAT and FPERT, H. Fuher, V. B. Kartha, P. J. Krueger and H. H. Mantsch, *Natl. Res. Counc. Can. Bull.*, 1976, **15**, 1.
36 A. J. Barnes, *J. Mol. Struct.*, 1984, **113**, 161.
37 M. M. Sokolova, V. V. Mel'nikov, V. A. Ostrovskii, G. I. Koldobskii, A. A. Mel'nikov and B. V. Gidaspov, *Zh. Org. Khim.*, 1975, **11**, 1744.
38 F. Billes, H. Endrédi and G. Keresztury, *J. Mol. Struct.* (*Theochem.*), 2000, **530**, 183.
39 F. G. Baglin, *J. Chem. Phys.*, 1972, **56**, 358.
40 M. T. S. Rosado, M. L. T. S. Duarte and R. Fausto, *J. Mol. Struct.*, 1997, **410–411**, 343.
41 S. Jarmelo, T. M. R. Maria, M. L. P. Leitão and R. Fausto, *Phys. Chem. Chem. Phys.*, 2000, **2**, 1155.